受入
86-4-333
高工研図書室

EUROPEAN ORGANIZATION FOR NUCLEAR RESEARCH

CERN-EP/86-35
March 13th, 1986

ANGULAR DISTRIBUTIONS OF MUON PAIRS PRODUCED BY 194 GeV/c NEGATIVE PIONS

NA10 Collaboration

S.Falciano[a], M.Guanziroli, H.Hofer, P.Le Coultre,
H.Suter, V.L.Telegdi and G.Viertel,
ETH, Zurich, Switzerland.

B.Betev[b] and K.Freudenreich[c],
CERN, Geneva, Switzerland.

A.Ereditato[d], E.Gorini[e] and P.Strolin,
Università di Napoli and INFN Sezione di Napoli, Naples, Italy.

P.Bordalo[f], L.Cerrito, L.Kluberg,
A.Romana, R.Salmeron and J.Varela[f],
Ecole Polytechnique, Palaiseau, France.

J.J.Blaising[g], A.Degré[g], P.Juillot,
R.Morand[g], B.Mours[g] and M.Winter,
CRN and Université Louis Pasteur, Strasbourg, France.

ABSTRACT

We present the angular distributions of muon pairs obtained in a high-statistics experiment using a 194-GeV/c π^--beam impinging on a tungsten target. Our results are based on the analysis of 145 000 events with positive Feynman x and mass above 4.07 GeV/c^2, excluding the Υ region. Simple first-order QCD relations allow us to determine the ratio of annihilation with gluon emission to the sum of annihilation and gluon Compton scattering, which is found to be about 58% to 75%. We determine the parton square intrinsic transverse momenta to be of the order of 0.6 (GeV/c)^2, and about 30% larger in the pion than in the nucleon. At large x_1, our data agree with the higher-twist hypothesis, and support the interpretation of the relevant scale parameter as the dimuon square transverse momentum.

(Submitted to Zeitschrift für Physik C, Particles and Fields)

---

a) Now at INFN Sezione di Roma, Rome, Italy.

b) Permanent address: Institute of Nuclear Research and Nuclear Energy, Sofia, Bulgaria.

c) Now at ETH, Zurich, Switzerland.

d) Now at CERN, Geneva, Switzerland.

e) Now at Universität München, Garching, FRG.

f) Now at CFMC-INIC, Lisbon, Portugal.

g) Now at LAPP, Annecy-le-Vieux, France.

1. Introduction

The angular distributions of the lepton pairs produced in hadronic interactions have long been recognized to provide information on the production mechanism complementary to that provided by other differential distributions. In particular, for the angular distributions, predictions can be made which are largely independent of the detailed parton distributions, and also insensitive to normalization.

In the framework of the parton model, hadronic lepton-pair production is described by the annihilation of a quark from one of the hadrons with an antiquark from the other hadron into a transversely polarized virtual photon, which then decays into a pair of leptons (Fig. 1a). This picture, the so-called "naïve" Drell-Yan [1] mechanism, reproduces fairly well the gross features of the data at low values of the transverse momentum P_T of the pair. It fails however to explain the absolute normalization, and the large number of events observed at high P_T. Inclusion of the intrinsic transverse momenta of the partons is not sufficient to reconcile the predictions with the data. On the other hand, the QCD processes to first order in the coupling constant α_s $q\bar{q} \rightarrow \gamma^* G$ (annihilation with gluon emission, Fig. 1b and 1c), and $qG \rightarrow \gamma^* q$ (gluon Compton scattering, Fig. 1d and 1e), where the momentum of the gluon balances the transverse momentum of the photon, reproduce the experimental P_T distributions fairly well. These predictions are however sensitive to the quark and gluon distributions, and the latters are outside the present predictive power of QCD.

The angular distribution predicted by the "naïve" Drell-Yan model is $1+\cos^2\theta$, where θ is the polar angle between the incoming hadrons and the decay leptons in the center-of-mass system of the latters. In QCD, the angular distributions will depend not only on θ, but also on the azimuthal angle ϕ, and will be described by three coefficients (aside from normalization). For the gluonic annihilation process, and in a particular reference frame, one of these coefficients is a function of kinematical variables only, i.e., independent of the parton distributions [2–5], while for the Compton scattering process it depends, but only weakly, on these distributions [3–7].

In the case of π^--nucleon interaction, higher-twist (i.e., non-perturbative) effects [8] (Fig. 1f and 1g) can become important at large value of the relative momentum x_1 of the antiquark, and give rise to longitudinally polarized photons, with a specific angular distribution.

Several published experiments [9 – 13] have given results on the polar distribution $1+\lambda\cos^2\theta$. These are all in agreement, within errors, with the "naïve" Drell-Yan prediction $\lambda = 1$, except at large x_1, where one experiment [10] confirmed the higher-twist prediction. More recently, an experiment [11, 12] gave results for the angular distributions in $\cos\theta$ and ϕ. However, its limited statistics does not allow to draw definite conclusions; in particular, no higher-twist effect was observed. Conversely, that effect was clearly seen in an other recent experiment [13]; on the other hand, the statistics were too low to see any departure from a uniform azimuthal distribution.

In the next section, we shall define the angles θ and ϕ in several reference frames, and give the relations between these frames. In the third section, we shall describe our experiment, the data selection, the Monte-Carlo, and the analysis procedure. The fourth section contains the results and the fifth one the comparison with the predictions from QCD. The last section contains our conclusions, and some kinematical relations are given in an appendix.

2. Reference frames and angle definitions

In the "naïve" Drell-Yan model, the transverse momentum of the partons is neglected, so that the partons move parallel to the colliding hadrons. In the center-of-mass system of the lepton pair, the partons are hence collinear, and the angular cross section of the pair is described by

$$(1/\sigma)d\sigma/d\Omega = [3/2(\lambda+3)]\ (1 + \lambda\cos^2\theta), \qquad (1)$$

where θ is the angle between the momentum $\vec{P}_\mu$ of one of the muons and the line of flight of the partons, and $\lambda = 1$. However, when the transverse momentum P_T of the photon is not neglected, the quark and antiquark momenta are not collinear any longer; one expects $\lambda < 1$, and the angular distribution will depend also on the azimuthal angle ϕ (Fig. 2).

The choice of axes in the center-of-mass system of the dilepton is arbitrary, and many special choices have been proposed. We shall restrict ourselves to the following three frames:

- $\hat{z}$ parallel to the beam momentum $\vec{P}_b$: this is the t-channel (or Gottfried-Jackson [14], GJ) frame;
- $\hat{z}$ antiparallel to the target momentum $\vec{P}_t$: this is the u-channel (UC) frame;

– $\hat{z}$ parallel to the bisector of $\vec{P}_b$ and $-\vec{P}_t$: this frame (CS) was proposed by Collins and Soper [15].

As we shall see, the theoretical predictions are especially simple when expressed in the CS frame. We choose $\hat{y}$ parallel to $\vec{P}_b \times \vec{P}_t$ and $\hat{x}$ (parallel to $\vec{P}_T$ in the CS frame) completes a right-handed frame. The polar angle θ is the angle between $\hat{z}$ and the momentum of the *positive* muon $\vec{P}_\mu$, and the azimuthal angle ϕ is the angle between $\hat{y}$ and $\hat{z} \times \vec{P}_\mu$.

The three frames defined above are related by a single rotation of angle β around their common $\hat{y}$ axis, where β is half the angle between $\vec{P}_b$ and $-\vec{P}_t$. The relation between the CS and the GJ frames, or between the UC and the CS frames is thus simply:

$$\begin{aligned} x' &= x\cos\beta + z\sin\beta, \\ y' &= y, \\ z' &= -x\sin\beta + z\cos\beta; \end{aligned} \tag{2}$$

the tangent of the angle β is a function of P_T and the mass M of the dilepton [15] [see Appendix, Eq. (A12)]:

$$\tan\beta = \rho, \tag{3}$$

where $\rho \equiv P_T/M$.

Averaging over the initial hadron polarizations, summing over the lepton spins, and applying invariance principles (permutation symmetry, gauge invariance, parity conservation, and unitarity), the most general form of the angular differential cross section reads [16, 17]:

$$(1/\sigma)(d\sigma/d\Omega) = [3/4\pi(\lambda+3)]\,[1 + \lambda\cos^2\theta + \mu\sin 2\theta\cos\phi + (\nu/2)\sin^2\theta\cos 2\phi], \tag{4}$$

where the coefficients λ, μ, and ν may in general be functions of the kinematical variables $\sqrt{s}$ (center-of-mass energy), M, P_T, x_F (relative longitudinal momentum of the dilepton), and x_1.

The angular differential cross section is often written using the notation proposed by Collins and Soper [15]:

$$\begin{aligned} (1/\sigma)d\sigma/d\Omega = (3/16\pi)[1 &+ \cos^2\theta + (A_0/2)(1-3\cos^2\theta) \\ &+ A_1\sin 2\theta\cos\phi + (A_2/2)\sin^2\theta\cos 2\phi]; \end{aligned} \tag{5}$$

the relation between λ, μ, and ν and A_0, A_1, and A_2 is: $\lambda = (2-3A_0)/(2+A_0)$, $\mu = 2A_1/(2+A_0)$, and $\nu = 2A_2/(2+A_0)$. While the latter parametrization is more convenient for theoretical calculations, the one defined by Eq. (4) is more suited for data analysis.

Using Eqs (2) and (3), one can write the coefficients in one frame as functions of the coefficients in an other frame [4, 18]:

$$\lambda' = [(1-\rho^2/2)\lambda + 3\rho\mu + 3\rho^2\nu/4]/\Delta,$$
$$\mu' = [-\rho\lambda + (1-\rho^2)\mu + \rho\nu/2]/\Delta, \qquad (6)$$
$$\nu' = [\rho^2\lambda - 2\rho\mu + (1+\rho^2/2)\nu]/\Delta,$$

with:

$$\Delta = 1 + \rho^2 + \rho^2\lambda/2 - \rho\mu - \rho^2\nu/4,$$

where λ, μ, and ν are the coefficients in the CS (UC) frames, and λ', μ', and ν' are the coefficients in the GJ (CS) frames. The inverse transformations (i.e., from the GJ to the CS frame or from the CS to the UC frame) are obtained by replacing ρ by $-\rho$ in Eqs (6).

It should be stressed that with Eqs (6) the choice of a reference frame looses most of its relevance when the angular distributions in both $\cos\theta$ and ϕ are measured, as one can easily compute the coefficients in any one frame, once they are known in another one; this choice becomes only a matter of convenience. This is not the case when only the $\cos\theta$ distribution is measured.

3. Experimental details

3.1 Set-up

The data used for this analysis were recorded in the NA10 experiment at the CERN SPS facility. The apparatus has been extensively described elsewhere [19], and we shall briefly recall its main features here. An unseparated beam of 194 GeV/c (95% π^-, 4.4% K^-, and 0.6% $\bar{p}$), with a 10% momentum bite and an average intensity of 1 to $2\cdot10^9$ particles per burst, was focussed on a high-purity tungsten target. To allow an estimation of the reinteraction effects, two different targets were used, with lengths 5.6 and 12 cm. The target was followed by a beam dump/hadron absorber, consisting of a uranium/tungsten core surrounded by a carbon/iron absorber. The distance between the target and the core of the dump (120 cm) was sufficiently large to avoid any contamination of our sample by pairs created in the dump. The dump/absorber was followed by a muon spectrometer. The analysis magnet had a hexagonal symmetry and produced a toroidal field. Only events whith both muons traversing the air sectors of the magnet were retained. For triggering purposes, two sets of two hodoscopes divided into sextants were installed in front and behind the magnet; the last hodoscope was located behind an iron

muon filter. The trajectories of the particles were delineated by two sets of four multiwire proportional chambers, one upstream and one downstream of the magnet; each chamber had three gaps with wire planes rotated by 60° with respect to each other.

A first-level trigger required at least one muon with transverse momentum larger than 0.8 GeV/c pointing to the target, in at least two different sextants. This first-level trigger suppressed the low-mass events. To further reduce the number of triggers, a second-level trigger, based on an event-buffer/microprocessor system [20], rejected events with high multiplicities or low masses.

The muon trajectories were reconstructed off-line using the information from the wire chambers and from the hodoscopes. An iterative algorithm determined the momentum of the muons to better than 2% accuracy. Corrections were made to account for the energy loss in the absorber and in the target. Additional off-line cuts [21], based on geometrical criteria, reduced the number of randomly associated tracks to a negligible level. As the size of the target was small compared to the vertex resolution, we constrained the vertex to the center of the target.

To eliminate the J/ψ- and Υ-family resonances, events with $M < 4.07$ GeV/c^2 and 8.5 GeV/c^2 $< M <$ 11 GeV/c^2 were rejected. Events with $x_F < 0$ were also rejected, in order to minimize reinteraction effects. After all cuts, our final sample consisted of some 145 000 opposite-sign dimuons. As the like-sign events represent only 0.3% of the opposite-sign events, no subtraction was made.

3.2 Monte-Carlo

The events simulated by the Monte-Carlo program were generated with a realistic P_T distribution [12], an (M, x_F) distribution essentially following the Buras-Gaemers [22] parametrization of the structure functions, a uniform ϕ distribution and a $1+\cos^2\theta$ distribution. The Fermi motion was taken into account following Ref. 23, with the high-momentum tail cut off at 0.4 GeV/c. The measured spatial and momentum distributions of the pion beam were folded in; the energy loss and multiple scattering in all parts of the apparatus were taken into account.

The Monte-Carlo events were processed through the *same* reconstruction program as the real data, and the same trigger requirements and selection criteria were imposed. The final Monte-Carlo sample consisted of over one million events.

3.3 Acceptance and resolution

The NA10 apparatus was not specifically designed for the study of the angular distributions, but rather for the determination of the parton distributions. The acceptance in $\cos\theta$ (Fig. 3a) is therefore not optimal, being peaked at $\cos\theta = 0$, and the range covered ($|\cos\theta| < 0.6$) is rather limited; on the other hand, the acceptance in ϕ (Fig. 3b) is more uniform, extending over the full range $-\pi$ to π. The coefficient λ of $\cos^2\theta$ in Eq. (4) is primarily determined by large values of $|\cos\theta|$, where we have few events; hence, our λ is rather inaccurately determined, and may suffer from biases. The coefficient μ of $\sin2\theta\cos\phi$ is determined mostly by the ϕ distribution at intermediate values of $|\cos\theta|$, and hence is also prone to biases. On the other hand, the coefficient ν of $\sin^2\theta\cos2\phi$ is sensitive to $\cos\theta$ values around zero, where our events are concentrated, and is quite well determined and little biased. In the comparison with the theory, we shall take advantage of the small uncertainty of ν.

The acceptances in M and P_T are slowly increasing with these variables [19], but the physical distributions drop rapidly, and there are few events above M_Υ or at high P_T. The acceptance in x_1, relevant for the study of the higher-twist effect, is ~9% at $x_1 \approx 0.4$ and falls below 1% at $x_1 \approx 1$, where the parton density also falls rapidly, thus making the investigation of the higher-twist effect with our data rather difficult.

The mass resolution was found, by a fit to the width of the Υ resonance [24], to be 3.3% at $M = M_\Upsilon$, in agreement with the Monte-Carlo prediction. The rms resolutions in $\cos\theta$ and ϕ, determined by Monte-Carlo, are $\Delta\cos\theta = 0.06$ (GJ), 0.03 (CS), and 0.04 (UC), and $\Delta\phi = 0.4$ for all three frames.

3.4 Analysis procedure

We determined the coefficients λ, μ, and ν in several intervals of the variables M, P_T, ρ, x_F, and x_1. For each interval, the ($\cos\theta$, ϕ) plane was divided in 20×20 bins; since the apparatus accepts only a limited range in $\cos\theta$, only between 200 and 250 of these bins were populated. For the interval $M > M_\Upsilon$, where we have comparatively few events, we used only 10×10 bins.

The coefficients were estimated by a standard least-squares method: we adjusted the Monte-Carlo generated angular distributions to the observed ones by a fit with seven parameters, viz.:

$$\Delta N/\Delta\Omega = N_0(1 + \lambda\cos^2\theta + \mu\sin2\theta\cos\phi + (\nu/2)\sin^2\theta\cos2\phi + \alpha\cos\theta + \beta\sin\theta\cos\phi + \gamma\sin\theta\sin\phi). \quad (7)$$

N_0 is an arbitrary normalization factor (we did not seek to determine here absolute cross sections); replacing N_0 by $N_0'/(3+\lambda)$ to take the denominator of the r.h.s. of Eq. (4) explicitly into account does not change the results of the fits.

The three parameters α, β, and γ multiply terms which are odd under inversion, i.e., under the transformation $\cos\theta \to -\cos\theta$, $\phi \to -\phi$. By comparing data taken with opposite field polarities, we found that most of this asymmetry can be ascribed to experimental effects not contained in the Monte-Carlo. The residual, i.e., field-independent, average asymmetry is parametrized by $\alpha = -0.06 \pm 0.03$, $\beta = -0.01 \pm 0.01$, and $\gamma = 0.01 \pm 0.01$, giving a global asymmetry of $(-3 \pm 1)\%$. Note that the physical asymmetry expected from electromagnetic corrections is predicted [25] to be $+1\%$ to $+1.5\%$ and that from electroweak interference [26, 27, 28] ranges from $+0.2\%$ at 4 GeV/c^2 to $+0.8\%$ at 8 GeV/c^2 [29].

We verified that the geometrical acceptance is insensitive to the fitted parameters. Neither the acceptance nor the smearing due to the finite resolution, which were taken into account in the Monte-Carlo, were iterated during the fitting procedure.

We checked that our results were neither affected by the choice of the binning, nor by the particular distributions chosen to generate the Monte-Carlo events. We obtained acceptable χ^2s in all intervals: the ratio χ^2 per degrees of freedom ranged from 0.8 to 1.2.

The coefficients were computed in the GJ, CS, and UC frames. As an illustration, we show in Fig. 4a the values of λ, μ, and ν for the five intervals (shown in Table 2) in P_T. As expected, the values for the three frames lie close to each other at low P_T, where ρ is small, but their differences increase with P_T. As the next step, we computed the values in the CS frame from the values in the GJ and UC frames, by means of the transformation Eqs (6), using the ρ appropriate to each specific interval. In Fig. 4b we display for each coefficient the three values in the CS frame, i.e., the one obtained directly and the other two computed as just indicated. The coefficient values lie now closer to each other, but still do not coincide: the remaining difference allows us to estimate the systematic uncertainties; we see that these uncertainties are comparable to the statistical errors, i.e., large for λ, and relatively small for μ and ν. In an attempt to reduce the systematic uncertainties, we computed a weighted mean of the three values; this procedure does of course not reduce the statistical errors: we assigned as the statistical error on the mean value the average of the statistical errors in each frame.

4. Results

We recall that our dimuon events were produced by a 194 GeV/c π^- beam impinging on a tungsten target; events with $x_F < 0$ or $M < 4.07$ GeV/c^2 were rejected, as well as events with 8.5 GeV/c^2 < M < 11 GeV/c^2, where the contribution of dimuons from Υ-family resonances amounts to about 25% [24]. We present below the values of the coefficients as functions of selected kinematical variables.

4.1 M dependence

The M dependence in the CS frame is given in Table 1 and in Fig. 5 (the values corresponding to the Υ region, i.e., the shaded interval on the figure, are shown for comparison). The coefficient λ increases slightly with M, while μ and ν decrease, although all points are compatible, within errors, with constant values, viz., $\langle\lambda\rangle = 0.69 \pm 0.05$, $\langle\mu\rangle = 0.007 \pm 0.012$, and $\langle\nu\rangle = 0.096 \pm 0.009$. Fitting only the $\cos\theta$ distribution, we find a slightly larger value for λ, viz., $\langle\lambda\rangle = 0.83 \pm 0.06$.

4.2 P_T dependence

The variation of the coefficients with P_T in the CS frame is given in Table 2 and in Fig. 6. The coefficient λ is compatible with a constant value; μ is constant and compatible with zero, while ν starts from zero and increases with P_T. In the limit $P_T = 0$, one expects indeed $\mu = 0$ and $\nu = 0$, i.e., the "naïve" Drell-Yan prediction; on the other hand, our data do not agree with the corresponding value $\lambda = 1$: we observe a significantly smaller value of λ in the first interval.

4.3 ρ dependence

The dependence on ρ, in the CS frame, given in Table 3 and in Fig. 7, is similar to the dependence on P_T. We give it here because this dimensionless variable plays an important role in the phenomenological discussion of our results.

4.4 x_F dependence

The x_F dependence of the coefficients in the CS frame is given given in Table 4 and in Fig. 8. While λ and μ are constant ($\langle\lambda\rangle = 0.76 \pm 0.05$ and $\langle\mu\rangle = 0.005 \pm 0.011$), ν increases slightly over the observed range.

A straight-line fit gives $\nu = (0.05 \pm 0.02) + (0.20 \pm 0.07) x_F$, with $\chi^2/\text{d.o.f.} = 0.9/3$. We are not aware of any QCD prediction for the variation of the angular distributions with x_F.

4.5 x_1 dependence

We give the x_1 dependence (Table 5 and Fig. 9) *in the GJ frame*, as the higher-twist predictions have been made for that frame. One sees that λ drops for x_1 above 0.6, as expected for this effect. On the other hand, the probability that the highest two points of λ, μ, and ν (i.e., for $x_1 > 0.6$) agree with their averages for $x_1 < 0.6$, is ~30%. Thus our data, although *consistent with* the higher-twist hypothesis, are not sufficient to *prove* it.

5. Comparison with theoretical predictions

5.1 Intrinsic transverse momentum

Motivated by the copious yield of dimuons observed at large P_T ($P_T > 0.5$ GeV/c), several early attempts were made to improve the "naïve" Drell-Yan model by including the parton intrinsic transverse momenta, but these did however neither suffice [30] to explain this yield, nor the observed dependence of $\langle P_T \rangle$ on $\sqrt{s}$. The high-P_T yield is by now well understood in the framework of QCD. Nevertheless, the parton intrinsic transverse momenta still play a role in the behaviour of the angular distributions [3, 15, 31, 32].

In the limit $P_T \to 0$, one expects the "naïve" Drell-Yan model to apply, and therefore the QCD corrections to be small in the low-P_T region. Neglecting these corrections, one obtains [3] for the first coefficient of the angular distribution, after smearing over the quark transverse momenta: $A_0 = 4\langle K_{1T}^2 \rangle / M^2$ in the GJ frame, and $A_0 = 4\langle K_{2T}^2 \rangle / M^2$ in the UC frame, where $\langle K_{1T}^2 \rangle$ ($\langle K_{2T}^2 \rangle$) are the mean square transverse momenta of the quarks in the pion (nucleon).

With the parametrization of Eq. (4), we get:

$$\langle K_{1T}^2 \rangle = M^2(1-\lambda)/2(\lambda+3) \qquad (8)$$

in the GJ frame, and the same relation for $\langle K_{2T}^2 \rangle$ in the UC frame. In the first P_T bin ($P_T < 0.5$ GeV/c) we have (Fig. 4a): $\lambda = 0.73 \pm 0.14$ (GJ frame), and $\lambda = 0.63 \pm 0.14$ (UC frame). From Eq. (8), with $\langle M^2 \rangle = 25.6$ (GeV/c^2)^2 in the first P_T bin, we obtain $\langle K_{1T}^2 \rangle = (0.9 \pm 0.5)$ (GeV/c)^2, and $\langle K_{2T}^2 \rangle = (1.3 \pm 0.5)$ (GeV/c)^2.

A better estimate of the difference between the square transverse momenta of the partons in the pion and in the nucleon can be obtained by investigating the ρ dependence of the coefficient μ. In the CS frame, this coefficient is proportional to the difference between the mean square transverse momenta of the annihilating partons [15]. Assuming that QCD contributions from both partons to the transverse momentum of the dimuon are the same, a departure of μ from zero in this frame can be ascribed to the difference between the *intrinsic* transverse momenta [15, 32]:

$$\mu(\rho) = -\rho(\langle K_{1T}^2\rangle - \langle K_{2T}^2\rangle)/(\langle K_{1T}^2\rangle + \langle K_{2T}^2\rangle). \quad (9)$$

Fitting the $\mu(\rho)$ distribution (Table 3), we obtain (Fig. 7):

$$(\langle K_{1T}^2\rangle - \langle K_{2T}^2\rangle)/(\langle K_{1T}^2\rangle + \langle K_{2T}^2\rangle) = 0.14 \pm 0.06, \quad (10)$$

with χ^2/d.o.f. = 4.1/4; the intrinsic square momentum of a parton is thus $(28 \pm 12)\%$ larger in a pion than in a nucleon; note that Eq. (9) is directly sensitive to the sign of the difference between the intrinsic transverse momenta in both hadrons, contrary to the estimates of $\langle K_{1T}^2\rangle$ and $\langle K_{2T}^2\rangle$ yielded by Eq. (8), which give an opposite sign for this difference.

The contribution ν_i of the intrinsic transverse momenta to ν is given by [15, 32]:

$$\nu_i(\rho) = \rho^2[(\langle K_{1T}^2\rangle - \langle K_{2T}^2\rangle)/(\langle K_{1T}^2\rangle + \langle K_{2T}^2\rangle)]^2; \quad (11)$$

for our highest point ($\rho \approx 0.5$) it amounts to only 0.005, compared to the measured value $\nu = 0.290 \pm 0.038$ (Table 3); it can therefore be neglected compared to the QCD contribution. This is not the case for the coefficient λ, which is more sensitive to the intrinsic transverse momenta; a comparison of ν and λ will allow us to determine again the parton intrinsic transverse momenta. A general prediction of the parton model, analogous to the Callan-Gross relation [33] in deep-inelastic scattering, is [2, 17, 34, 35]:

$$1 - \lambda = 2\nu. \quad (12)$$

This relation, valid for spin-1/2 quarks, is insensitive to first-order QCD corrections [36]. It is however modified by the quark transverse momenta, which affect the two sides of Eq. (12) differently: one obtains, as a function of M in the CS frame [32]:

$$1 - \lambda(M) = 2\nu(M) + (8/M^2)\,\langle K_{1T}^2\rangle\langle K_{2T}^2\rangle / (\langle K_{1T}^2\rangle + \langle K_{2T}^2\rangle). \quad (13)$$

A fit of $\lambda(M)$ to the data (Table 1), with $\nu(M)$ given by QCD (see section 5.2 below), yields (Fig. 5):

$$\langle K_{1T}^2\rangle\langle K_{2T}^2\rangle/(\langle K_{1T}^2\rangle + \langle K_{2T}^2\rangle) = (0.28 \pm 0.16)\ (\mathrm{GeV/c})^2 \quad (14)$$

(we rejected the events at $x_1 > 0.6$ to eliminate possible higher-twist effects, see section 5.3 below; the

fit shown in Fig. 5 was made without this cut). Combining Eqs (14) and (10), we obtain $\langle K_{1T}^2 \rangle = (0.66 \pm 0.38)$ (GeV/c)^2 and $\langle K_{2T}^2 \rangle = (0.50 \pm 0.29)$ (GeV/c)^2, in agreement, within the large errors, with the estimates given by Eq. (8).

These values of $\langle K_T^2 \rangle$ are considerably larger than those currently envisaged in theoretical papers (see e.g. Ref. 37 and 38). However, recent theoretical improvements, like soft-gluon resummation, are not included in the present analysis; it has been shown [38] that these improvements reduce the amount of intrinsic transverse momentum needed to reproduce the observed P_T distributions.

For the distributions integrated over M, we shall use Eq. (13) averaged over $1/M^2$, viz. numerically

$$1 - \lambda = 2\nu + 0.12. \tag{15}$$

5.2 First-order QCD corrections

We now turn to the first-order QCD corrections to the Drell-Yan picture. In the leading-twist approximation, the lepton-pair production is described, in addition to the zeroth-order Drell-Yan process ($q\bar{q} \to \gamma^*$, Fig. 1a), by quark-antiquark annihilation with hard-gluon emission ($q\bar{q} \to \gamma^* G$, Fig. 1b and 1c), and by quark-gluon scattering (hard-gluon Compton scattering, $qG \to \gamma^* q$, Fig. 1d and 1e). Vertex corrections of order α_s^2 give also first-order contributions through interference with the zeroth-order diagram; however, soft-gluon resummation, which takes these vertex corrections into account, modifies the first-order contributions to the angular distribution coefficients only slightly [28, 39]. Together, these corrections largely account for the dimuon production at high P_T, for the dependence of P_T on $\sqrt{s}$, and for the factor of about two to three (K-factor) between the measured cross sections and those predicted by the "naïve" Drell-Yan model.

Knowing the parton distributions both in the pion and in the nucleon, one can compute the ratio of the hard-gluon annihilation contribution to the sum of the hard-gluon annihilation and Compton scattering contributions. In the next-to-leading approximation to order α_s [40] and subtracting the soft-gluon resummation term [41], and taking the same structure functions as in Ref. 42, we obtain for this ratio a value between 70% and 85% for M above 4 GeV/c^2 (this computation also indicates that these two diagrams contribute for some 10% only to the total cross section). This result is little sensitive to the particular choice of structure functions and varies slowly with P_T [43]. On the other hand,

we can *measure* this ratio almost independently of the structure functions by using the kinematical dependence of the angular distribution coefficients.

For the annihilation as well as for the Compton scattering, the partial angular cross section at the parton level reads [34]:

$$(1/\sigma)d\sigma/d\Omega = (3/16\pi)[1 + (E_1^2\cos^2\theta_1 + E_2^2\cos^2\theta_2)/(E_1^2 + E_2^2)], \quad (16)$$

where $E_i = |\vec{P}_i|$ is the energy of parton i (i = 1,2), and θ_i the angle between $\vec{P}_i$ and $\vec{P}_\mu$. Neglecting the intrinsic transverse momenta, the partons lie in the plane of the hadrons, and one has: $\vec{P}_i = (P_{ix}, 0, P_{iz})$; with $\vec{P}_\mu = (M/2)(\sin\theta\cos\phi, \sin\theta\sin\phi, \cos\theta)$, one obtains: $E_i^2\cos^2\theta_i = (P_{ix}\sin\theta\cos\phi + P_{iz}\cos\theta)^2$. Substituting in Eq. (16) and comparing with Eq. (5), one gets:

$$A_0 = A_2 = (P_{1x}^2 + P_{2x}^2)/(E_1^2 + E_2^2), \quad (17)$$

and

$$A_1 = (P_{1x}P_{1z} + P_{2x}P_{2z})/(E_1^2 + E_2^2). \quad (18)$$

For the annihilation, $P_1 = x_1P_b$ and $P_2 = x_2P_t$; with the expressions for E_b, $\vec{P}_b$, E_t, and $\vec{P}_t$ given in the Appendix [Eqs (A9), (A15), and (A16)], one obtains, in the CS frame [2 – 5]:

$$A_0 = A_2 = \rho^2/(1+\rho^2), \quad (19)$$

which is *independent* of the parton densities, and:

$$A_1 = [-\rho/(1+\rho^2)][(x_1e^{-y} - x_2e^{y})/(x_1e^{-y} + x_2e^{y})], \quad (20)$$

where $y = (1/2)\ln[(E + P_L)/(E - P_L)]$ is the rapidity of the dimuon in the center-of-mass system of the hadrons, and P_L its longitudinal momentum. A_1 *can not be made independent* of the parton densities; it is however expected [3] to be small: at zero rapidity, it is proportional to the relative difference between the quark densities in the beam and target hadrons. Moreover, averaging over the dimuon longitudinal momenta, it has been shown [5, 7] that, *in the GJ frame*: $A_0 = A_2 = 2\rho^2/(1+\rho^2)^2$, and $A_1 = -\rho(1-\rho^2)/(1+\rho^2)^2$, which, transformed to the CS frame, give Eq. (19) and $A_1 = 0$.

For the Compton scattering, the situation is more involved, as one has to distinguish between the case where the gluon comes from the pion: $P_1 = x_2P_t$, $P_2 = x_1P_b + x_2P_t$, and the case where it comes from the nucleon: $P_1 = x_1P_b$, $P_2 = x_1P_b + x_2P_t$. This leads to expressions for $A_0 = A_2$ and A_1 which are not symmetric in x_1 and x_2 [3 – 7, 44], and therefore are not functions of ρ only. However, averaging over the dimuon longitudinal momentum, one finds [5, 7] *in the GJ frame*: $A_0 = A_2 = 6\rho^2/(1+\rho^2)(1+5\rho^2)$; *assuming* $A_1 = 0$ in the CS frame, i.e., that the average contributions from both partons to P_T are equal, one obtains:

$$A_0 = A_2 = 5\rho^2/(1+5\rho^2), \tag{21}$$

in this frame, also independently of the parton densities.

As we have seen in section 5.1, λ is affected by intrinsic transverse momentum contributions, which are negligible for ν, and, in addition, ν is expected to be less biased than λ (see section 3.3); we shall therefore apply the relations above to ν. For the latter, Eq. (19) and (21) give respectively, in the CS frame:

$$\nu_{q\bar{q}}(\rho) = 2\rho^2/(2+3\rho^2), \tag{22}$$

and:

$$\nu_{qG}(\rho) = 10\rho^2/(2+15\rho^2). \tag{23}$$

Combining linearly these two terms, and assuming that there is no other contribution to ν, we can write:

$$\nu(\rho) = \alpha\nu_{q\bar{q}}(\rho) + (1-\alpha)\nu_{qG}(\rho). \tag{24}$$

Fitting $\nu(\rho)$ to our data (Table 3), we find $\alpha = 0.58 \pm 0.08$, with $\chi^2/\text{d.o.f.} = 1.9/4$ (Fig. 7). We also fitted $\nu(P_T)$ to the data (Table 2), replacing ρ^2 by $\langle 1/M^2 \rangle P_T^2$ in Eqs (22) and (23), with $\langle 1/M^2 \rangle = 0.043$ $(\text{GeV}/c^2)^{-2}$. This fit yields $\alpha = 0.64 \pm 0.07$, with $\chi^2/\text{d.o.f.} = 3.5/4$ (Fig. 6). Similarly, we fitted $\nu(M)$ to the data (Table 1), replacing ρ^2 by $\langle P_T^2 \rangle / M^2$ in Eqs (22) and (23), with $\langle P_T^2 \rangle = 1.60$ $(\text{GeV}/c)^2$; we find $\alpha = 0.75 \pm 0.06$, with $\chi^2/\text{d.o.f} = 3.0/4$. The ratio of first-order annihilation to first-order annihilation and Compton scattering lies thus in the range 58% to 75%, a value slightly smaller, but still in agreement with our calculated value. Strictly speaking, Eqs (22) and (23) are not valid over the full P_T range, as the first-order QCD corrections diverge in the limit $P_T \to 0$; nevertheless, Eq. (24) reproduces well our data, down to the smallest values of P_T.

We have seen that the relation $\lambda(M) = 1 - 2\nu(M)$, Eq. (12), with $\nu(M)$ given by QCD, fits nicely the data, provided one allows for an additional intrinsic transverse momentum contribution. Averaging over $1/M^2$, we can also compare Eq. (15) to the variation of λ with ρ (Fig. 7), or with P_T (Fig. 6); whereas the points at $\rho \leq 0.3$, or $P_T \leq 2$, agree with this relation, the points at higher values are larger than expected. The innaccuracy in the determination of λ (see section 3.3) does not suffice to explain this discrepancy.

5.3 Spin of the gluon

The QCD predictions given in the preceding section for vector gluons can be adapted to the case of scalar gluons [7, 34, 45]. The vector-like character of the gluon has been established by the e^+e^- experiments at Petra [29]. Nevertheless, we verified this result by fitting our data to the first-order QCD predictions for scalar gluons [7]. For a scalar gluon and *in the GJ frame* (to avoid using the formula given for μ, which diverges at $\rho = 0$, when transforming the predictions to the CS frame), one finds for hard-gluon annihilation:

$$\nu_{q\bar{q}}(\rho) = 2/(2\rho^2 + 3), \tag{25}$$

and for Compton scattering:

$$\nu_{qG}(\rho) = 2\rho^2/(1 + 3\rho^2 + \rho^4). \tag{26}$$

As these predictions are valid only for relatively large values of ρ [7], we fitted the last three points in ρ (i.e. $\rho > 0.2$) to $\nu(\rho) = \alpha\nu_{q\bar{q}}(\rho) + (1-\alpha)\nu_{qG}(\rho)$; we find $\alpha = 0.17 \pm 0.03$, but with χ^2/d.o.f. = 15.4/2, giving a probability smaller than $5 \cdot 10^{-4}$ for a scalar gluon.

5.4 Higher twist

Higher-twist effects in QCD (i.e. non-scaling terms characterized by a Q^{-2n} behaviour) arise, among other cases, when more than the minimum number of partons are involved in the initial state. This happens in $\pi N \to \mu\mu X$ when the annihilating antiquark carries a large fraction of the pion momentum, i.e. when $x_1 \to 1$ [8]. This antiquark is then far off-shell, and has to be considered bound. This bound state can be represented by a single gluon exchange between the annihilating quark or antiquark and the pion spectator quark (Fig. 1f and 1g). The dimuon production process can no longer be described by the annihilation of two free quarks; the zero spin of the pion influences the angular distributions, which now acquire a $\sin^2\theta$ term specific of a longitudinal photon polarization [8]:

$$(1/\sigma)d\sigma/d\Omega = \{3/8\pi[(3+\lambda')\sigma_T/2 + \sigma_L]\}\,[\sigma_T(1+\lambda'\cos^2\theta) + \sigma_L\sin^2\theta + (\sigma_{LT}/2)\sin 2\theta\cos\phi], \tag{27}$$

where σ_T, σ_L, as well as the interference term $\sigma_{LT} = \sqrt{(\sigma_L\sigma_T)}$ are functions of x_1. The factor λ' provides for the fact that λ is not necessarily 1 at low x_1; the term in $\sin^2\theta\cos 2\phi$, which is not enhanced by the higher-twist effect, is not given here. Comparing Eq. (27) with Eq. (4), one obtains:

$$\lambda(x_1) = (\sigma_T - \sigma_L)/(\sigma_T + \sigma_L), \tag{28}$$

and

$$\mu(x_1) = \sigma_{LT}/2(\sigma_T + \sigma_L). \tag{29}$$

The pion structure function is also modified by the higher-twist effect, and becomes [8, 13]:

$$F_\pi(x_1) \sim x_1^{\alpha}[(1-x_1)^{\beta}+\eta^2], \tag{30}$$

with:

$$\eta^2 = (4/9)\kappa^2/M^2, \tag{31}$$

where κ^2 is a scale parameter; note that η^2 has the M^{-2} dependence specific of a twist-4 effect.

Integrating Eq. (27) and comparing with Eq. (30), one obtains:

$$\sigma_T \sim x_1^{\alpha}(1-x_1)^{\beta}, \tag{32}$$

and

$$\sigma_L \sim \eta^2 x_1^{\alpha}; \tag{33}$$

substituting σ_T and σ_L in Eqs (28) and (29), one obtains:

$$\lambda(x_1) = [\lambda'(1-x_1)^{\beta}-\eta^2]/[(1-x_1)^{\beta}+\eta^2], \tag{34}$$

and

$$\mu(x_1) = -(1-x_1)^{\beta/2}/2[(1-x_1)^{\beta}+\eta^2]. \tag{35}$$

We determined λ' and η^2 by fitting Eqs (34) and (35) simultaneously to the λ and μ distributions, with $\beta = 1.0$ determined by our experiment [42]; we found $\lambda' = 0.72 \pm 0.05$ and $\eta^2 = 0.033 \pm 0.007$, with χ^2/d.o.f$= 8.0/8$ (Fig. 9). With $\langle M^2 \rangle = 26.3$ (GeV/c^2)^2, we get $\kappa^2 = (2.0 \pm 0.4)$ (GeV/c)^2. Although Eq. (27) is not supposed to be valid at low x_1, it reproduces our data over the full x_1 range well. We nevertheless checked our result by performing the same fit to the last three points only (i.e. $x_1 > 0.5$): we obtained $\lambda' = 0.70 \pm 0.14$ and $\eta^2 = 0.022 \pm 0.012$, with χ^2/d.o.f. $= 6.4/4$. With $\langle M^2 \rangle = 39.7$ (GeV/c^2)^2 for this interval, we obtain again $\kappa^2 = (2.0 \pm 1.1)$ (GeV/c)^2. The value of κ^2 is close to our value $\langle P_T^2 \rangle = 1.60$ (GeV/c)^2; this is in agreement with the interpretation of κ^2 as the mean square transverse momentum of the dimuon, as proposed by the authors of Ref. 8. Note that Fermilab experiment 615 [13], working at a pion momentum of 80 GeV/c, found $\kappa^2 = (0.62 \pm 0.16)$ (GeV/c)^2, also in agreement with their value $\langle P_T^2 \rangle = 0.56$ (GeV/c)^2.

As mentionned above, there is no higher-twist prediction for ν; although the relation $1-\lambda = 2\nu$ is not supposed to hold in this case, it nevertheless agrees well with the observed ν distribution, with χ^2/d.o.f. $= 4.8/5$ (Fig. 9).

In the leading-twist approximation, the coefficients λ, μ, and ν are not expected to vary strongly with x_1 [39]. Fixing the coefficients at constant values in the CS frame ($\lambda = 0.76$, $\mu = 0$, and $\nu = 0.10$),

and transforming to the GJ frame with Eqs (6), we obtain the dot-dashed curves shown in Fig. 9. A χ^2-test gives a 16% probability for λ to agree with this assumption, but only a 2% probability for μ and a 0.1% probability for ν; the combined probability is only $3 \cdot 10^{-4}$, compared to a 46% probability for the higher-twist fit combined with Eq. (15).

6. Conclusions

We have presented the angular distributions of some 145 000 dimuons, the highest statistics used in such an analysis sofar. The coefficient μ was found to be small in the CS frame, indicating that the annihilating quarks contribute about equally to the dimuon transverse momentum. Using Eq. (12), analogous to the Callan-Gross relation, and the small departure of μ from zero (CS frame), we computed the squared parton intrinsic transverse momenta to be (0.66 ± 0.38) $(\mathrm{GeV/c})^2$ in the pion and (0.50 ± 0.29) $(\mathrm{GeV/c})^2$ in the nucleon, with a relative difference of $(28 \pm 12)\%$. The good accuracy of the coefficient ν allowed us to measure the ratio of first-order hard-gluon annihilation over hard-gluon annihilation and Compton scattering, which was found to amount to 58%-75%, slightly smaller but consistent with the value of 70%-85% calculated using currently known structure functions. The relation $1 - \lambda = 2\nu$, with an additional term due to intrinsic transverse momenta, agrees with our data at moderate values of ρ, or P_T, but fails at larger values.

Our data at large x_1 are consistent with the higher-twist prediction, although not sufficient to prove it, and we found support for the interpretation of the relevant scale parameter κ^2 as the dimuon mean square transverse momentum.

In summary, first-order perturbative QCD, taking into account the parton intrinsic transverse momenta and the higher-twist effect at large x_1, provides a coherent description of the dimuon angular distributions.

Acknowledgements

One of us (H.S.) wishes to thank Drs E.L. Berger, P. Chiappetta, Y. Gabellini and especially J. Cleymans for enlightning discussions. We thank Prof. D.A. Jensen for a contribution to this work.

Appendix

We recall here some useful kinematical relations. In the hadronic center-of-mass system, and neglecting the masses, one has:

$$\vec{P}_t^{\,*} = -\vec{P}_b^{\,*}, \quad E_t^{\,*} = E_b^{\,*}, \tag{A1}$$

where $E_b^{\,*}$, $\vec{P}_b^{\,*}$ are the energy and momentum of the beam hadron, and $E_t^{\,*}$, $\vec{P}_t^{\,*}$ those of the target hadron. The total energy squared is $s \equiv (P_b^{\,*} + P_t^{\,*})^2$, where $P_b^{\,*}$ and $P_t^{\,*}$ are the four-momenta of the hadrons. With Eq. (A1):

$$s = (E_b^{\,*} + E_t^{\,*})^2, \quad E_b^{\,*} = E_t^{\,*} = |\vec{P}_b^{\,*}| = |\vec{P}_t^{\,*}| = \sqrt{s}/2, \tag{A2}$$

and

$$P_b^{\,*} = (\sqrt{s}/2)(1, 0, 0, 1), \quad P_t^{\,*} = (\sqrt{s}/2)(1, 0, 0, -1); \tag{A3}$$

hence:

$$P_b^{\,*} P_t^{\,*} = s/2. \tag{A4}$$

The four-momentum of the dilepton is, in the hadronic center-of-mass system:

$$Q^* = (E^*, P_T^{\,*}, 0, P_L^{\,*}). \tag{A5}$$

The dilepton center-of-mass system, defined by $Q = (M, 0, 0, 0)$, is obtained through a Lorentz transformation along $\vec{Q}^*$, with $\vec{\beta} = \vec{Q}^*/E$, and $\gamma = E/M$ (as no confusion is possible we drop the stars on the dilepton variables E, P_T, P_L and y):

$$E_{b,t} = \gamma(E_{b,t}^{\,*} - \vec{\beta}\cdot\vec{P}_{b,t}^{\,*}); \tag{A6}$$

with Eq. (A3):

$$E_b = (\sqrt{s}/2M)(E - P_L), \quad E_t = (\sqrt{s}/2M)(E + P_L). \tag{A7}$$

Introducing the rapidity y of the dilepton in the hadronic center-of-mass system:

$$y \equiv (1/2)\ln[(E + P_L)/(E - P_L)] = \ln[(E + P_L)/\sqrt{(M^2 + P_T^{\,2})}], \tag{A8}$$

one obtains finally, with $\rho \equiv P_T/M$:

$$E_b = (\sqrt{s}/2)\sqrt{(1+\rho^2)}e^{-y}, \quad E_t = (\sqrt{s}/2)\sqrt{(1+\rho^2)}e^{y}. \tag{A9}$$

The angle 2β between the beam direction and the opposite to the target direction is given by:

$$\cos 2\beta = -(\vec{P}_b\cdot\vec{P}_t)/(E_b E_t); \tag{A10}$$

with $E_b E_t = (s/4)(1+\rho^2)$ and $\vec{P}_b\cdot\vec{P}_t = E_b E_t - P_b P_t = -(s/4)(1-\rho^2)$, using the invariant relation, Eq. (A4), one gets:

$$\cos 2\beta = (1-\rho^2)/(1+\rho^2); \tag{A11}$$

as $\cos 2\beta = (1-\tan^2\beta)/(1+\tan^2\beta)$, one has finally:

$$\tan\beta = \rho. \tag{A12}$$

In the GJ frame, the hadron momenta are:

$$\vec{P}_b = E_b(0, 0, 1), \tag{A13}$$

$$\vec{P}_t = E_t(-\sin 2\beta, 0, -\cos 2\beta) = E_t[-2\rho/(1+\rho^2), 0, -(1-\rho^2)/(1+\rho^2)]; \tag{A14}$$

in the CS frame:

$$\vec{P}_b = E_b(-\sin\beta, 0, \cos\beta) = E_b(-\rho/\sqrt{(1+\rho^2)}, 0, 1/\sqrt{(1+\rho^2)}], \tag{A15}$$

$$\vec{P}_t = E_t(-\sin\beta, 0, -\cos\beta) = E_t(-\rho/\sqrt{(1+\rho^2)}, 0, -1/\sqrt{(1+\rho^2)}]; \tag{A16}$$

and in the UC frame:

$$\vec{P}_b = E_b(-\sin 2\beta, 0, \cos 2\beta) = E_b[-2\rho/(1+\rho^2), 0, (1-\rho^2)/(1+\rho^2)], \tag{A17}$$

$$\vec{P}_t = E_t(0, 0, -1). \tag{A18}$$

References

[1] S.D. Drell and T.M. Yan, Phys. Rev. Lett. **25** (1970) 316; Ann. Phys. (NY) **66** (1971) 578.

[2] J.C. Collins, Phys. Rev. Lett. **42** (1979) 291.

[3] J. Cleymans and M. Kuroda, Nucl. Phys. **B155** (1979) 480.

[4] J. Lindfors, Physica Scripta (Sweden) **20** (1979) 19.

[5] R.L. Thews, Phys. Rev. Lett. **43** (1979) 987, 1968 (E).

[6] J. Cleymans and M. Kuroda, Phys. Lett. **80B** (1979) 385.

[7] R.L. Thews, Phys. Lett. **100B** (1981) 339.

[8] E.L. Berger and S.J. Brodsky, Phys. Rev. Lett. **42** (1979) 940; E.L. Berger, Phys. Lett. **89B** (1980) 241; Z. Phys. C, Particles and Fields **4** (1980) 289; S.J. Brodsky, E.L. Berger, and G.P. Lepage, *Proceedings of the Drell Yan Workshop,* Fermilab (1982), p.187, and references therein.

[9] K.J. Anderson et al., Phys. Rev. Lett. **42** (1979) 944; R. Barate et al., Phys. Rev. Lett. **43** (1979) 1541; C. Kourkoumelis et al., Phys. Lett. **91B** (1980) 475; D. Antreasyan et al., Phys. Rev. Lett. **45** (1980) 863; M. Corden et al., Phys. Lett. **96B** (1980) 417.

[10] K.J. Anderson et al., Phys. Rev. Lett. **43** (1979) 1219.

[11] J. Badier et al., Z. Phys. C, Particles and Fields **11** (1981) 195.

[12] O. Callot, *Thèse de doctorat d'Etat*, Orsay Report LAL 81/05 (1981), unpublished.

[13] S. Palestini et al., Phys. Rev. Lett. **55** (1985) 2649; S. Palestini, *Ph.D. dissertation*, Princeton University (1984), unpublished.

[14] K. Gottfried and J.D. Jackson, Nuovo Cim. **33** (1964) 309.

[15] J.C. Collins and D.E. Soper, Phys. Rev. **D16** (1977) 2219.

[16] R.J. Oakes, Nuovo Cim. **44A** (1966) 440.

[17] C.S. Lam and W.K. Tung, Phys. Rev. **D18** (1978) 2447.

[18] E.N. Argyres and C.S. Lam, Phys. Rev. **D26** (1982) 114.

[19] L. Anderson et al., Nucl. Instr. Methods **223** (1984) 26.

[20] J. Lecoq et al., Nucl. Instr. Methods **A237** (1985) 547.

[21] B. Betev et al., Z. Phys. C, Particles and Fields **28** (1985) 9.

[22] A.J. Buras and K.J.F. Gaemers, Nucl. Phys. **B132** (1978) 249.

[23] A. Bodek and J.L. Ritchie, Phys. Rev. **D23** (1981) 1070.

[24] S. Falciano et al., Phys. Lett. **158B** (1985) 92.

[25] D.L. Preston, Nucl. Phys. **B201** (1982) 383.

[26] R.W. Brown, K.O. Mikaelian and M.K. Gaillard, Nucl. Phys. **B75** (1974) 112.

[27] M. Chaichian, M. Hayashi, and K. Yamagishi, Phys. Rev. **D25** (1982) 130.

[28] M. Chaichian, M. Hayashi, and K. Yamagishi, Phys. Rev. **D26** (1982) 3078.

[29] For experimental results in e^+e^- collisions see e.g. S.L. Wu, Phys. Reports **107** (1984) 59.

[30] See e.g. M. Glück and E. Reya, Nucl. Phys. **B145** (1978) 24.

[31] E.L. Berger, J.T. Donohue, and S.Wolfram, Phys. Rev. **D17** (1978) 858.

[32] J. Cleymans and M. Kuroda, Phys. Lett. **105B** (1981) 68.

[33] C.G. Callan and D.J. Gross, Phys. Rev. Lett. **22** (1969) 156.

[34] K. Kajantie, J. Lindfors, and R. Raitio, Phys. Lett. **74B** (1978) 384; Nucl. Phys. **B144** (1978) 422.

[35] C.S. Lam and W.K. Tung, Phys. Lett. **80B** (1979) 228.

[36] C.S. Lam and W.K. Tung, Phys. Rev. **D21** (1980) 2712.

[37] A. Nakamura, G. Pancheri and Y.N. Srivastava, Z. Phys. C, Particles and Fields **21** (1984) 243.

[38] G. Altarelli, R.K. Ellis and G. Martinelli, Phys. Lett. **151B** (1985) 457.

[39] P. Chiappetta and T. Grandou, Z. Phys. C, Particles and Fields **25** (1984) 55.

[40] J. Kubar et al., Nucl. Phys. **B175** (1980) 251.

[41] Y. Gabellini et al., Nucl. Phys. **B211** (1983) 509.

[42] B. Betev et al., Z. Phys. C, Particles and Fields **28** (1985) 15.

[43] G. Altarelli et al., Nucl. Phys. **B246** (1984) 12.

[44] M. Noman and S.D. Rindani, Phys. Rev. **D19** (1979) 207.

[45] P.W. Johnson and W.K. Tung, Phys. Rev. Lett. **45** (1980) 1382.

Table 1: Coefficients λ, μ, and ν in the CS frame as a function of M

Interval	Events ($\times 10^3$)	⟨M⟩	ρ	λ	μ	ν
4.07 – 4.5	39.8	4.26	0.253	0.61±0.09	0.039±0.025	0.115±0.017
4.5 – 5.5	54.4	4.94	0.222	0.68±0.08	0.027±0.021	0.095±0.015
5.5 – 6.5	28.0	5.94	0.186	0.76±0.12	0.003±0.028	0.082±0.021
6.5 – 8.5	22.2	7.29	0.153	0.82±0.14	−0.062±0.028	0.087±0.023
8.5 – 11.0	7.8	9.44	0.118	0.70±0.23	−0.028±0.045	0.085±0.039
11.0 – 16.0	0.7	11.83	0.096	0.49±0.70	−0.038±0.147	0.002±0.125

Table 2: Coefficients λ, μ, and ν in the CS frame as a function of P_T

Interval	Events ($\times 10^3$)	$\langle P_T \rangle$	ρ	λ	μ	ν
0.0 – 0.5	26.9	0.32	0.063	0.68±0.14	0.037±0.024	−0.005±0.020
0.5 – 1.0	48.5	0.75	0.146	0.61±0.10	−0.034±0.020	0.035±0.015
1.0 – 1.5	35.8	1.23	0.238	0.90±0.09	−0.040±0.023	0.114±0.018
1.5 – 2.0	19.4	1.72	0.333	0.75±0.13	−0.040±0.042	0.220±0.028
2.0 – 6.0	14.5	2.52	0.491	0.90±0.12	−0.029±0.051	0.271±0.035

Table 3: Coefficients λ, μ, and ν in the CS frame as a function of ρ

Interval	Events ($\times 10^3$)	⟨ρ⟩	ρ	λ	μ	ν
0.0 – 0.1	30.2	0.064	0.064	0.74±0.13	0.013±0.023	−0.015±0.019
0.1 – 0.2	49.8	0.149	0.149	0.64±0.10	−0.032±0.021	0.051±0.015
0.2 – 0.3	33.6	0.245	0.245	0.66±0.11	−0.017±0.030	0.120±0.020
0.3 – 0.4	17.1	0.344	0.344	1.00±0.13	−0.118±0.048	0.197±0.031
0.4 – 1.2	14.3	0.514	0.514	0.91±0.13	−0.037±0.055	0.290±0.038

Table 4: Coefficients λ, μ, and ν in the CS frame as a function of x_F

Interval	Events ($\times 10^3$)	$\langle x_F \rangle$	ρ	λ	μ	ν
0.0 – 0.1	25.7	0.06	0.222	0.61±0.18	0.023±0.041	0.057±0.022
0.1 – 0.2	40.8	0.15	0.214	0.61±0.09	−0.002±0.022	0.090±0.017
0.2 – 0.3	38.7	0.25	0.212	0.85±0.08	0.003±0.018	0.096±0.017
0.3 – 0.4	24.5	0.34	0.211	0.94±0.12	0.031±0.025	0.108±0.021
0.4 – 1.0	15.4	0.48	0.197	0.47±0.21	−0.041±0.042	0.157±0.027

Table 5: Coefficients λ, μ, and ν in the GJ frame as a function of x_1

Interval	Events ($\times 10^3$)	$\langle x_1 \rangle$	ρ	λ	μ	ν
0.0 – 0.35	48.3	0.30	0.233	0.66±0.08	−0.095±0.020	0.093±0.016
0.35 – 0.50	65.7	0.42	0.213	0.61±0.06	−0.125±0.016	0.112±0.013
0.50 – 0.60	19.9	0.54	0.193	0.78±0.15	−0.085±0.033	0.163±0.024
0.60 – 0.70	7.8	0.64	0.172	0.23±0.26	−0.181±0.056	0.139±0.038
0.70 – 1.10	3.5	0.77	0.142	0.04±0.49	−0.075±0.097	0.171±0.057

Figure Captions

Figure 1 Diagrams contributing to the Drell-Yan cross section; a: lowest order; b, c: first-order annihilation with gluon emission; d, e: first-order gluon Compton scattering; f, g: higher-twist contributions to the photon polarization.

Figure 2 Definition of the angles θ and ϕ in the center-of-mass system of the dimuon. The reference frame shown here is the Collins-Soper frame.

Figure 3 Spectrometer acceptance as a function of the two angular variables $\cos\theta$ (a), and ϕ (b), as computed by Monte-Carlo.

Figure 4 Coefficients λ, μ, and ν as functions of P_T. (a) In the three different frames. Full circles: CS frame; open squares: GJ frame; open triangles: UC frame. (b) In the CS frame. Full circles: obtained in the CS frame; open squares: values from the GJ frame transformed to the CS frame; open triangles: values from the UC frame transformed to the CS frame. The squares and triangles are slightly displaced for clarity.

Figure 5 Coefficients λ, μ, and ν as a function of M in the CS frame. The horizontal bars give the size of each interval. For ν, the solid line corresponds to the fit to Eq. (24), and for λ to the fit to Eq. (13). The shaded interval corresponds to the Υ region and is omitted in the fit.

Figure 6 Coefficients λ, μ, and ν as a function of P_T in the CS frame. The horizontal bars give the size of each interval. For ν, the solid line is the result of the fit to Eq. (24), for λ it is given by Eq. (15).

Figure 7 Coefficients λ, μ, and ν as a function of ρ in the CS frame. The horizontal bars give the size of each interval. For μ, the dot-dashed line is the result of the fit to Eq. (9); for ν, the solid line is the result of the fit to Eq. (24), and for λ it is given by Eq. (15).

Figure 8 Coefficients λ, μ, and ν as a function of x_F in the CS frame. The horizontal bars give the size of each interval. The solid lines represent the simple fits described in Section 4.4.

Figure 9 Coefficients λ, μ, and ν as a function of x_1 in the GJ frame. The horizontal bars give the size of each interval. For λ and μ the solid lines are the results of the simultaneous fit to Eqs (34) and (35) (higher-twist effect), and for ν it is given by Eq. (15). The dot-dashed lines correspond to the leading-twist approximation, assuming λ and ν constant and $\mu = 0$ in the CS frame.

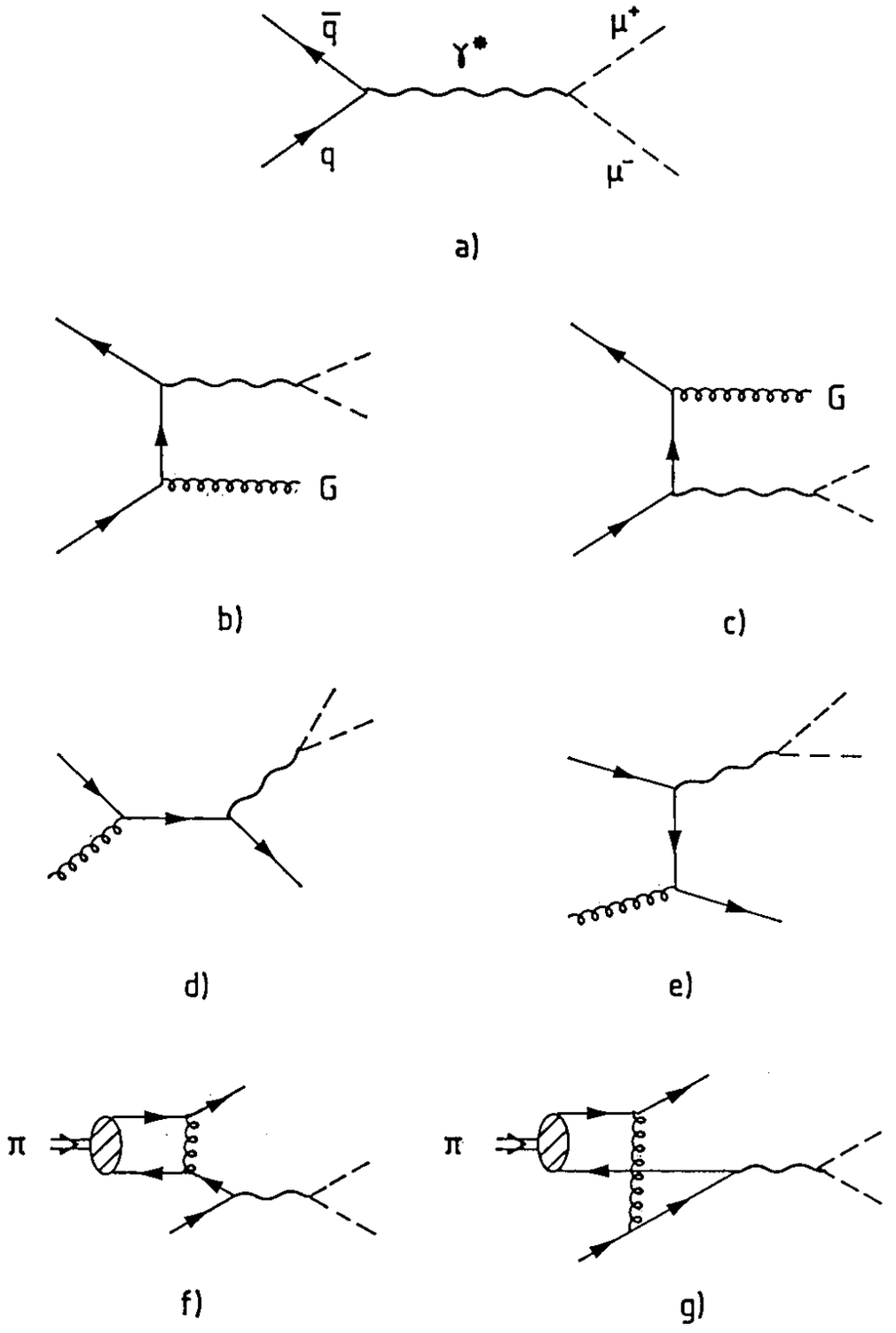

Figure 1

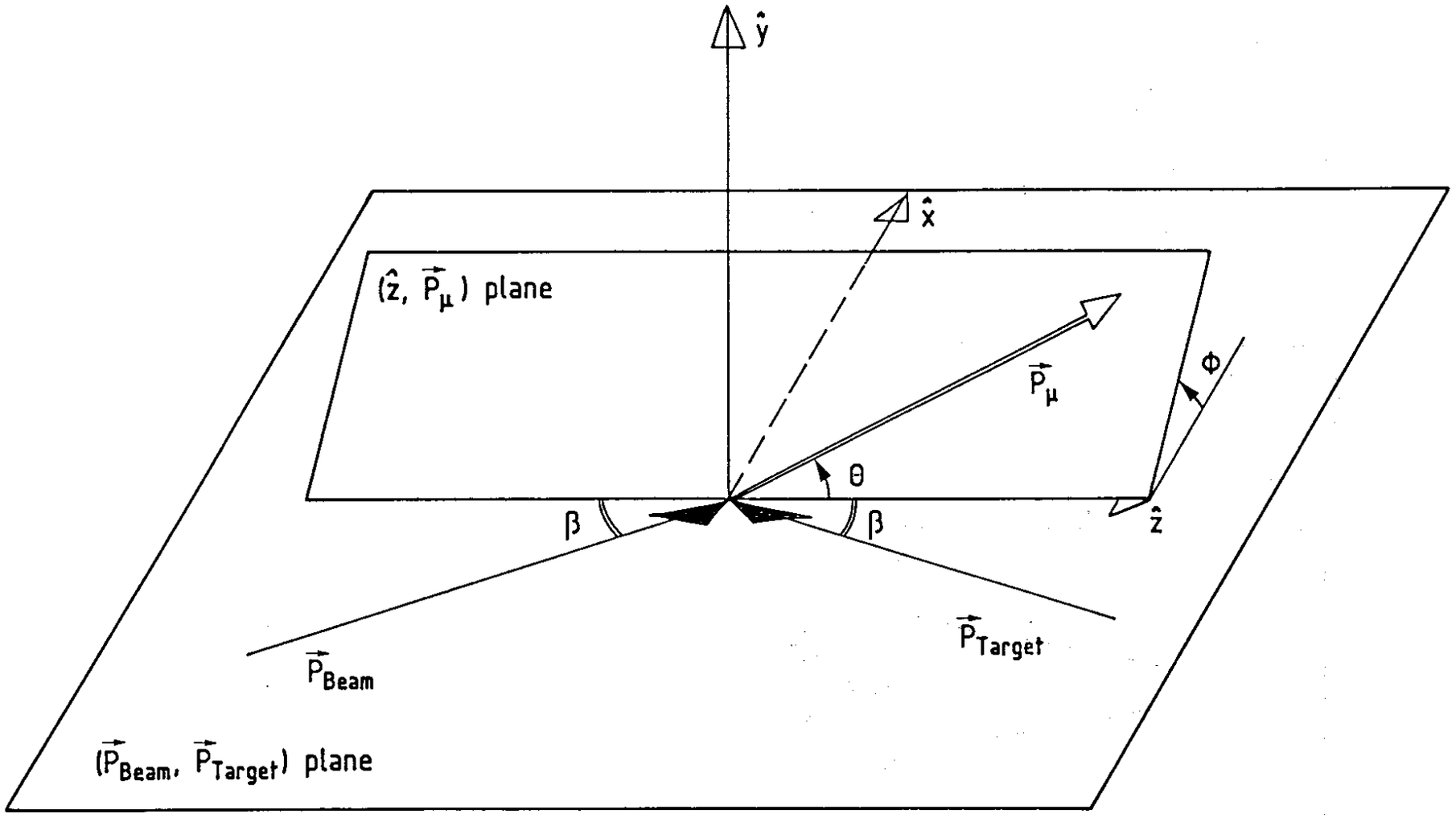

Figure 2

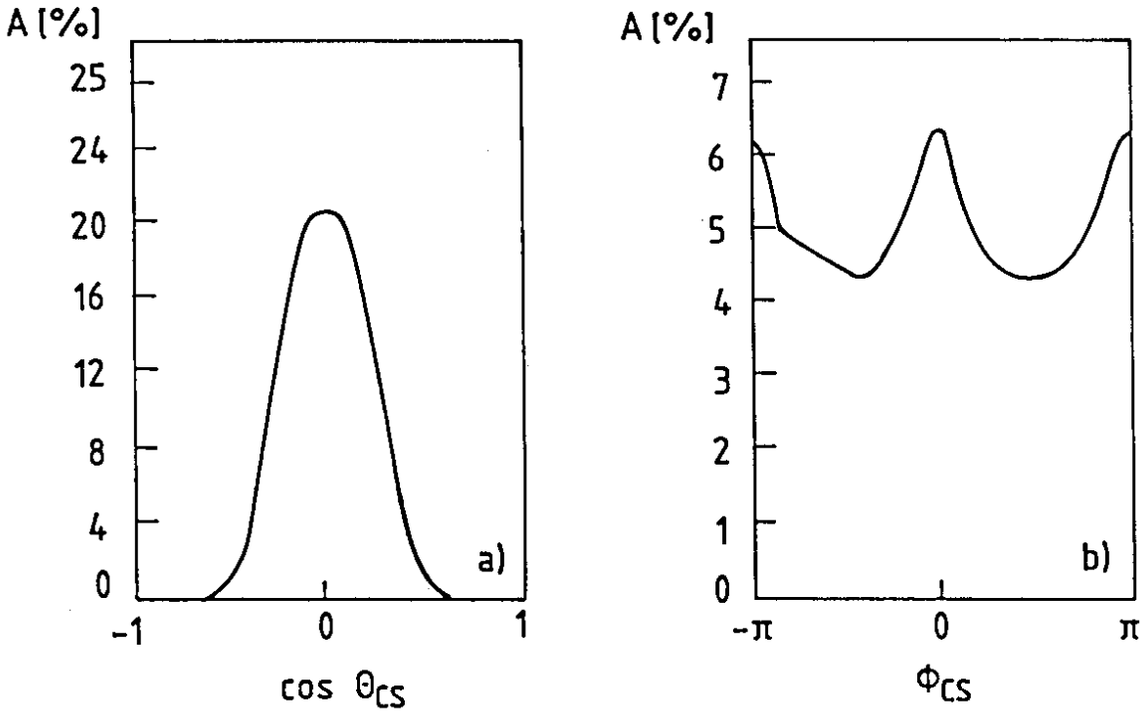

Figure 3

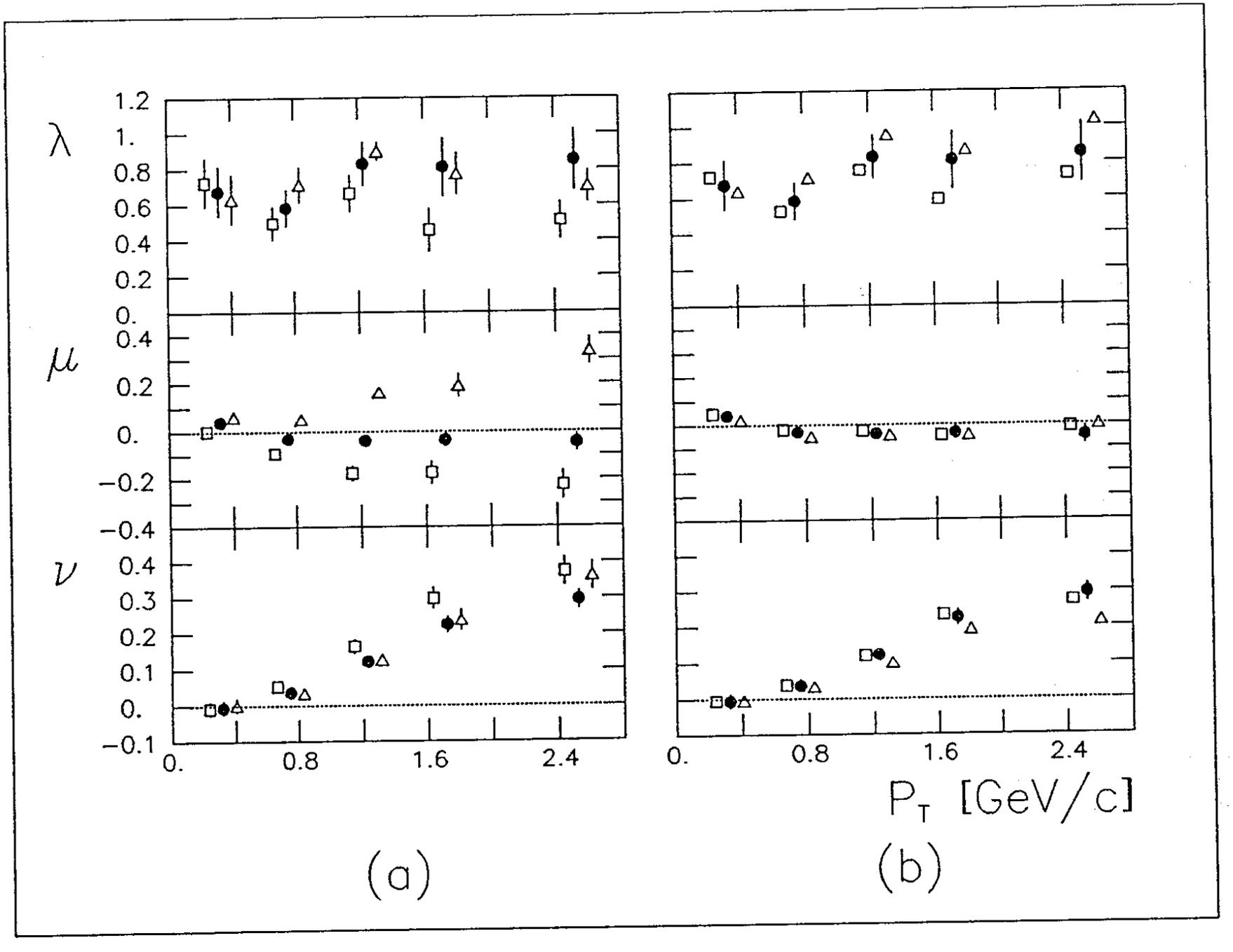
λ
μ
ν
1.2
1.
0.8
0.6
0.4
0.2
0.
0.4
0.2
0.
−0.2
−0.4
0.4
0.3
0.2
0.1
0.
−0.1
0.
0.8
1.6
2.4
0.
0.8
1.6
2.4
P_T [GeV/c]
(a)
(b)

Figure 4

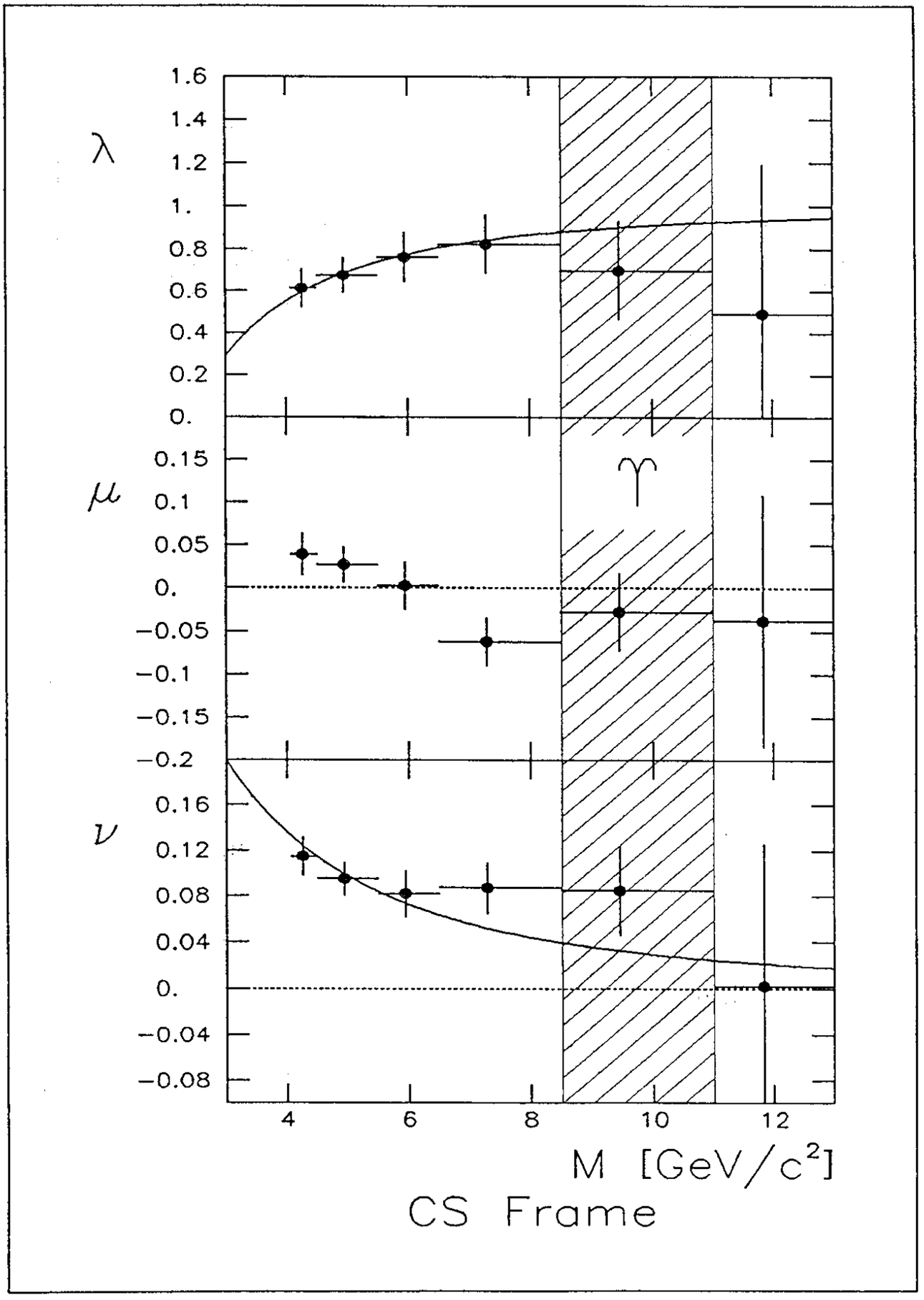
λ
μ
ν
Υ
1.6
1.4
1.2
1.
0.8
0.6
0.4
0.2
0.
0.15
0.1
0.05
0.
−0.05
−0.1
−0.15
−0.2
0.16
0.12
0.08
0.04
0.
−0.04
−0.08
4
6
8
10
12
M [GeV/c²]
CS Frame

Figure 5

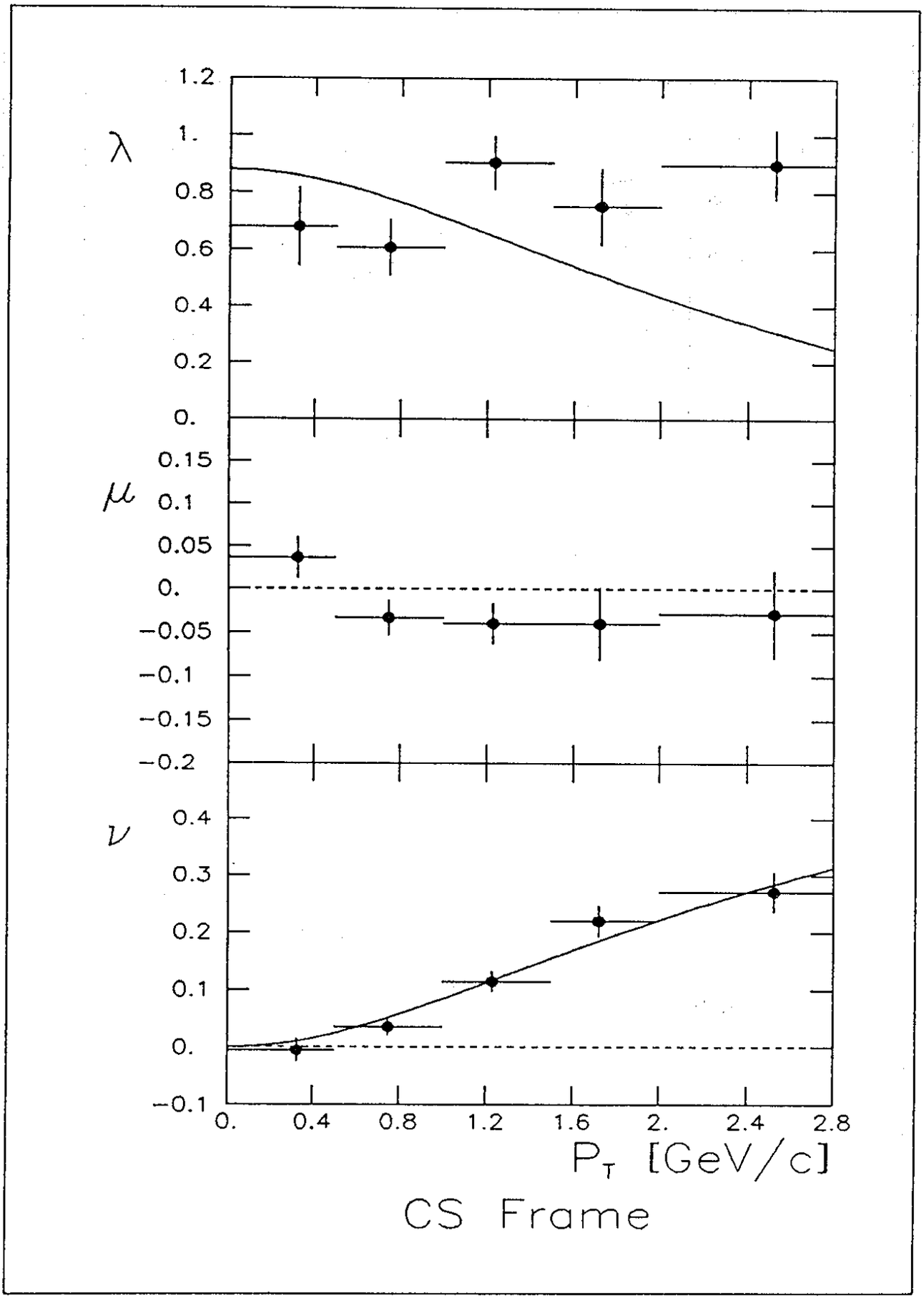
λ
μ
ν
1.2
1.
0.8
0.6
0.4
0.2
0.
0.15
0.1
0.05
0.
−0.05
−0.1
−0.15
−0.2
0.4
0.3
0.2
0.1
0.
−0.1
0.
0.4
0.8
1.2
1.6
2.
2.4
2.8
P_T [GeV/c]
CS Frame

Figure 6

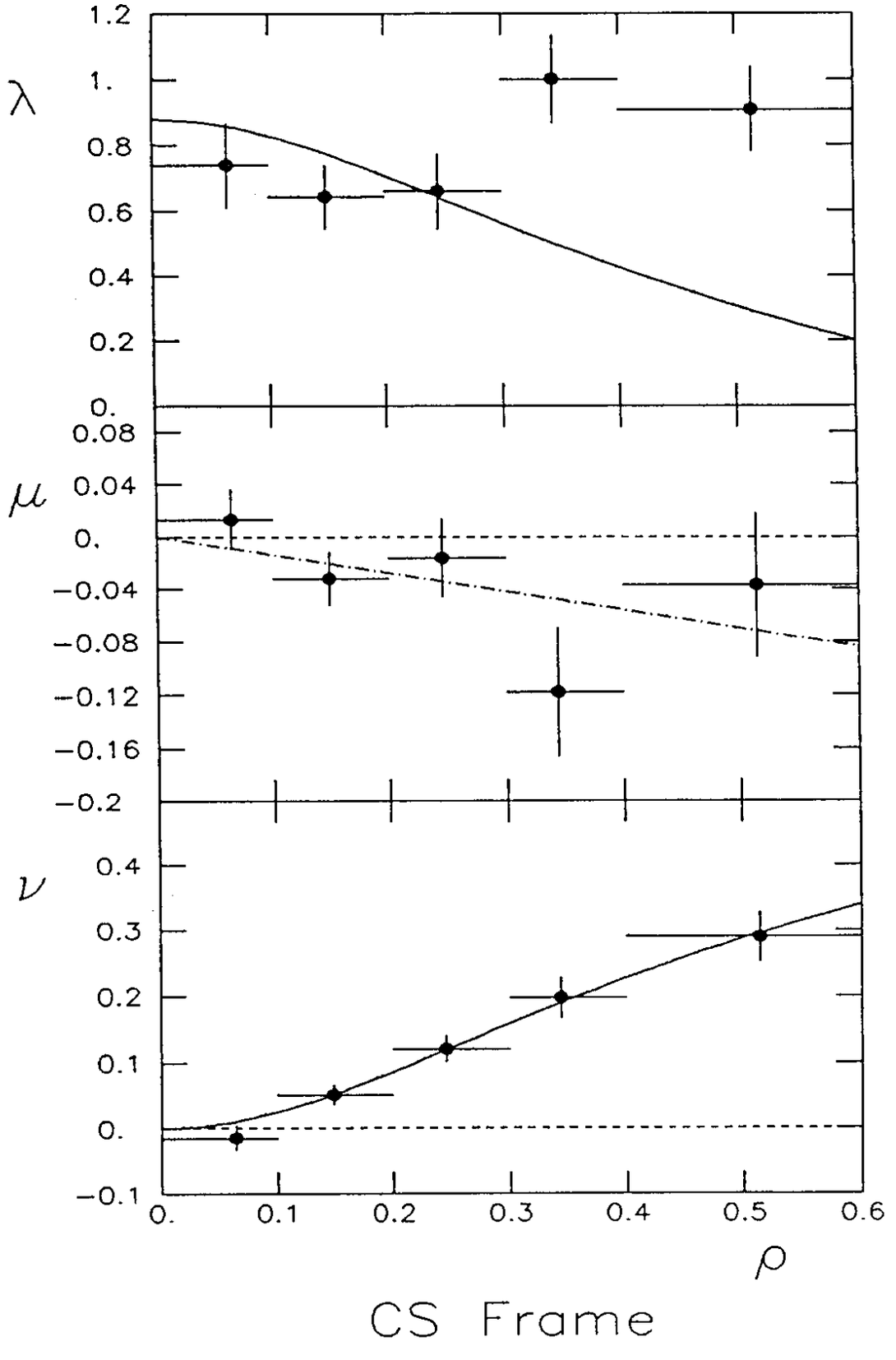

Figure 7

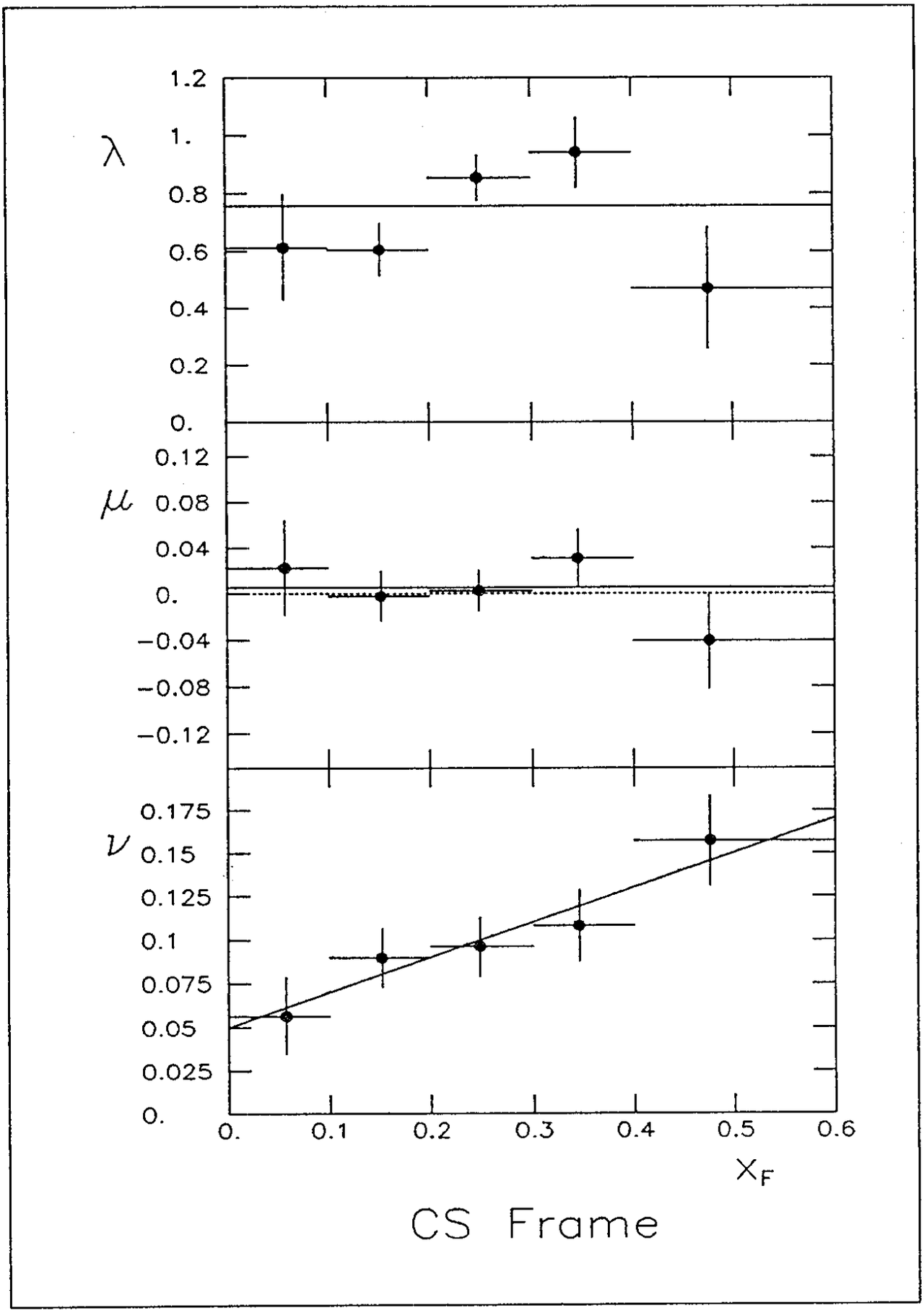
λ
1.2
1.
0.8
0.6
0.4
0.2
0.
μ
0.12
0.08
0.04
0.
−0.04
−0.08
−0.12
ν
0.175
0.15
0.125
0.1
0.075
0.05
0.025
0.
0.
0.1
0.2
0.3
0.4
0.5
0.6
X_F
CS Frame

Figure 8

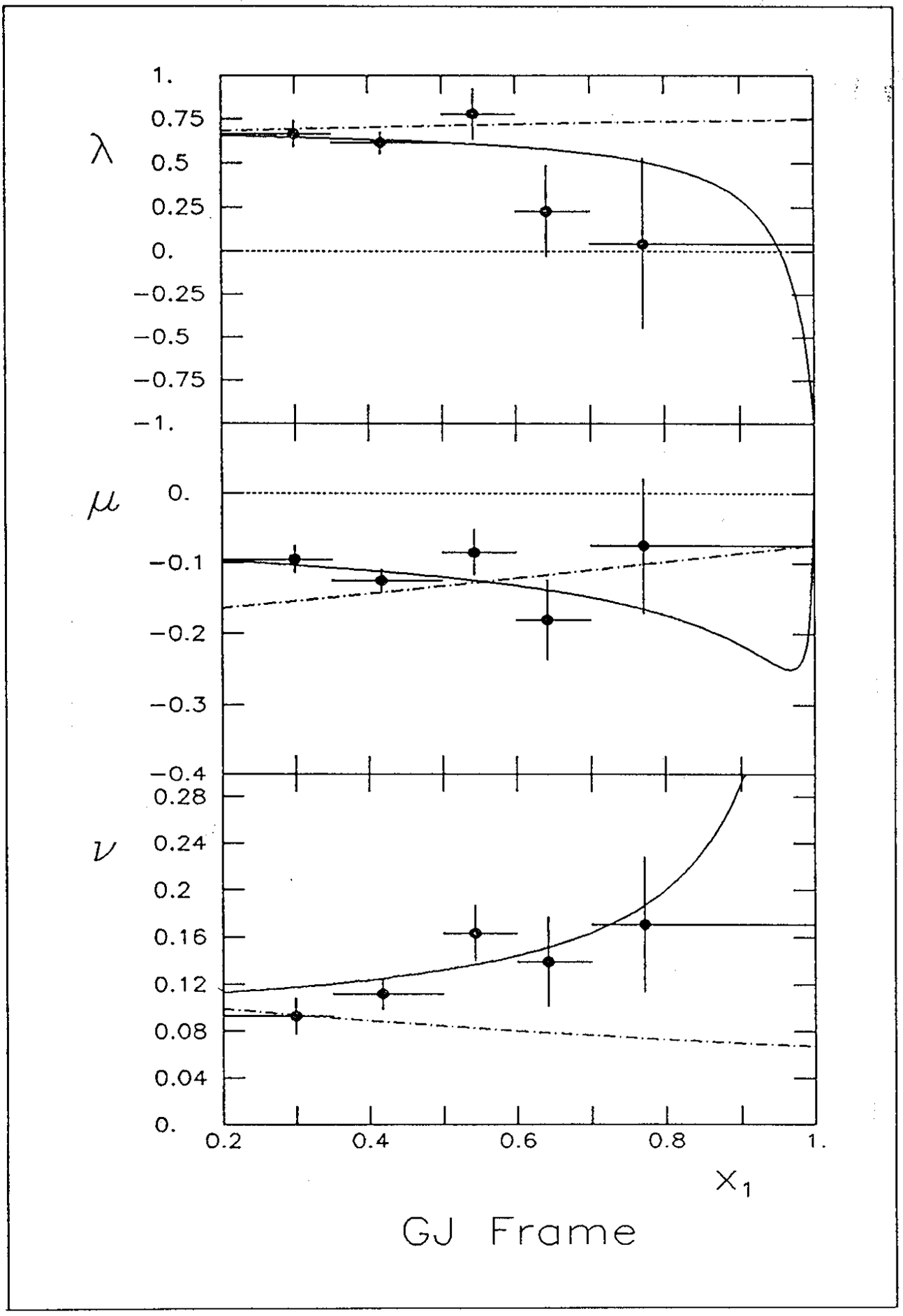
λ
μ
ν
1.
0.75
0.5
0.25
0.
−0.25
−0.5
−0.75
−1.
0.
−0.1
−0.2
−0.3
−0.4
0.28
0.24
0.2
0.16
0.12
0.08
0.04
0.
0.2
0.4
0.6
0.8
1.
X1
GJ Frame

Figure 9